Modeling the Dehydrogenation of Soot in Laminar Premixed Flames with a Multivariate Soot Particle Description

Achim Wick[1,*], *Heinz Pitsch*[1]

[1]Institute for Combustion Technology, RWTH Aachen University, Aachen, Germany

Abstract

A multivariate soot model in combination with Monte Carlo simulations is applied to a series of 1D laminar premixed burner-stabilized methane, ethylene, and benzene flames. The model is able to predict the soot yield with good accuracy. To evaluate if the model correctly captures the relative contribution of soot mass growth by condensation of polycyclic aromatic hydrocarbons and by acetylene addition by surface reactions, the H/C ratio is computed. It is shown that the dehydrogenation of the soot particles as well as the soot yield can be well predicted when the surface growth rate is increased, while the coagulation efficiencies of dimer formation from the gas phase are reduced.

1 Introduction

Modeling the formation of soot in flames is a challenging task both from a physical/chemical and from a mathematical/numerical point of view. The reason is that soot formation is an interplay of complex gas-phase chemical kinetics, particle dynamics, heterogeneous chemical reactions and influences of the flow field such as scalar mixing. The resulting soot particles differ significantly in size, mass, morphology, chemical composition and reactivity. A predictive model must be able to accurately describe the various chemical and physical processes that lead to the formation and growth of particles as well as the interaction between the gas phase and the particulate phase. As not every single particle can be tracked in a simulation, a statistical approach is required. The statistical information of the soot particle population is embodied in its Number Density Function (NDF), which is governed by a Population Balance Equation (PBE). The focus here is on the development of the physical/chemical soot model component, while Monte Carlo (MC) simulations are chosen as the statistical approach in order to eliminate the statistical error. This enables an effective assessment of the physical/chemical model.

The predictive capability of soot models is often evaluated based on the comparison of the predicted soot volume fraction or soot yield to experimental measurements. While the soot yield is certainly a very important figure of merit, its correct prediction for a specific case does not necessarily imply that the complex chemical and physical processes involved in soot formation are well captured by the model. However, capturing correctly the contribution of the different soot formation and growth processes is crucial for the model to be applicable to a wide range of operating conditions, fuels, and combustion regimes. The present work aims to contribute to the development of such a more general soot model by starting from a multivariate soot particle description and by also including the chemical composition of the particles as a target for model predictions.

The majority of existing soot models describes the particles by a single parameter, usually its mass or volume. While inceptive particles are nearly spherical, mature particles are clusters of so-called primary particles, which have a much larger surface area than spherical particles with the same volume [1]. Hence, the surface area is somewhat independent of the volume of a particle. This effect has been accounted for in the bivariate model by Mueller *et al.* [2], which describes the soot particles by their volume and surface area (VS model). Furthermore, particles which have the same volume and surface area, might have a very different chemical composition, depending on their age and how they were formed. Of particular importance is the chemical reactivity of the soot particles' surface. In a model developed by Blanquart and Pitsch [3, 4], the reactivity, described by the number of hydrogenated sites on the soot particle surface, is introduced as a third independent parameter (VSH model). This approach forms the baseline model applied here.

The mass growth of particles can be categorized into two classes of processes: growth due to the deposition of polycyclic aromatic hydrocarbons (PAH) onto the soot particle, and growth by heterogeneous surface reactions, which are mostly modeled by the H-abstraction-C_2H_2-addition (HACA) mechanism [5, 6]. The H/C ratio, i.e. the number of hydrogen atoms divided by the number of carbon atoms contained in a soot particle, depends on the relative contribution of these two processes. Hence, this quantity is identified to assess the model's ability to correctly capture the extent to which the predicted soot yield

* Corresponding author: a.wick@itv.rwth-aachen.de

is a result of PAH-based and acetylene-based growth. The VSH model has been extended by a model for the H/C ratio [3], which is passively computed, i.e. it does not influence the source terms of the various particle growth mechanisms.

To assess the model, a combined evaluation of the soot yield and the H/C ratio is performed for six 1D laminar premixed burner-stabilized flames. These include two methane, two ethylene, and two benzene flames. In these flames, the H/C ratio decreases with the height above the burner, indicating the dehydrogenation of the soot particles.

In the following section, the VSH model, the submodel for the H/C ratio, and the Monte Carlo code are briefly explained. Then, the results for the six laminar flames are presented and analyzed. The sensitivity of the predicted H/C ratio towards the relative contribution of PAH-based and acetylene-based growth is then studied. Based on this analysis, updated rates for the growth processes are proposed, and the updated model is validated for a larger set of 1D laminar premixed flames.

2 Multivariate soot model

The soot model includes five processes [2–4]: particle nucleation through dimerization of PAH and subsequent collision of these dimers, condensation of dimers onto the soot particle surface, surface growth by heterogeneous surface reactions, particle coagulation, and oxidation by OH and O_2. These processes are now described independently of the statistical description in the context of the VSH formulation. Subsequently, the MC algorithm is briefly outlined.

2.1 VSH formulation

Soot particles are assumed to form upon collision of two dimers, which each consists of two PAH molecules. Thus, the volume of the new particle is that of two dimers, and its surface area is calculated based on the assumption that the small particles are spherical. The hydrogen atoms are assumed to be all located on the surface of the particle. The soot density is assumed to be $1800\,\mathrm{kg/m^3}$.

The nucleation rate depends on the formation rate of dimers, which is proportional to the collision rate of PAH in the gas phase, multiplied by a coagulation efficiency, also referred to as sticking coefficient. It can be considered as a probability that two PAH will stick together and form a dimer upon collision. The seven PAH species included in the dimerization process are listed in Table 1. Compared to the suggestions made in [3, 4], naphthalene (A2) is excluded from the list, and the coagulation efficiency of P2 is reduced to better correspond to the value for A2R5, which has approximately the same mass as P2.

The soot particles can grow by collision with a dimer, which is then deposited onto the surface of the particle. This process is often referred to as condensation. The volume of the particle increases by the volume of a dimer.

When two particles coagulate, the total soot volume remains constant, while the volume of the new particle is the sum of the volumes of the two colliding particles.

Heterogeneous surface reactions are assumed to follow the HACA mechanism [5, 6], with the elementary reaction rates as suggested in [4] and references therein. Hence, the number of hydrogen atoms on the surface of the particle remains unchanged, while the volume increases by the volume of two carbon atoms. Furthermore, oxidation by OH and O_2 removes carbon atoms from the soot particle. For more information, including details on the functions for the changes of surface area and number of hydrogenated surface sites for the different processes, the reader is referred to the literature [3, 4].

Table 1: PAH species included in the dimerization model and their H/C ratio and assumed coagulation efficiency γ_i in the baseline model, cf. [3, 4].

Species	Formula	H/C	γ_i
Acenaphthylene (A2R5)	$C_{12}H_8$	0.667	0.0030
Biphenyl (P2)	$C_{12}H_{10}$	0.833	0.0032
Phenanthrene (A3)	$C_{14}H_{10}$	0.714	0.0150
Acephenanthrylene (A3R5)	$C_{16}H_{10}$	0.625	0.0250
Pyrene (A4)	$C_{16}H_{10}$	0.625	0.0250
Fluoranthene (FLTN)	$C_{16}H_{10}$	0.625	0.0250
Cyclopenta[cd]pyrene (A4R5)	$C_{18}H_{10}$	0.556	0.0390

2.2 H/C ratio

Different from the surface reactivity, the evaluation of the H/C ratio requires the knowledge of the volumetric hydrogen content, i.e. the number of all hydrogen atoms in a soot particle. Incipient soot particles formed during nucleation have as many hydrogen atoms as two dimers. Condensation increases the number of hydrogen atoms by the number of hydrogen atoms contained in one dimer, while surface growth does not change the number of hydrogen atoms in a particle. During coagulation, the total number of hydrogen atoms remains constant, and the number of hydrogen atoms in the new particle is the sum of the hydrogen atoms of the colliding particles.

2.3 Monte Carlo simulation

As diffusion of soot particles is negligible, the Population Balance Equation for the soot NDF reduces to an ordinary differential equation in time if the unsteady and convective terms are combined in a Lagrangian formulation. The flames considered here are one-dimensional, and the height above the burner can be transferred into a pseudo-time using the gas velocity. The NDF is then integrated in pseudo-time using a Monte Carlo method.

For the simulations presented here, 10^5 stochastic particles are used. During each time step, first the time is computed that it takes until the next process, also referred to as event, occurs. Then, the type of event, i.e. nucleation, condensation, coagulation, surface growth, or oxidation, is determined based on the rates of the different events. Once the event type is known, the particle which takes place in the event is chosen. For details of the algorithm, the reader is referred to the literature [7–12]. To increase the computational efficiency, the method of majorant kernels [7, 11] is applied to the coagulation process.

3 Baseline simulation results for 1D laminar premixed flames

Computational results for six 1D laminar premixed burner-stabilized flames are presented and compared to experimental data in this section. The soot model as described in the previous section is applied here. The performance of this baseline model is evaluated in terms of the soot yield, i.e. the fraction of the carbon content contained in the fuel that is transformed into soot, and the H/C ratio of the soot particles. The operating conditions of the flames are given in Table 2.

Table 2: Mixture composition, equivalence ratio ϕ, and cold gas velocity v_0 of the six laminar premixed flames. Flame parameters and experimental data from [13–20].

Flame	Fuel	X_{fuel}	$X_{\mathrm{O_2}}$	$X_{\mathrm{N_2}}$	ϕ	v_0
LT-M	CH_4	54.5	45.5	0.0	2.4	4 cm/s
HT-M	CH_4	54.5	45.5	0.0	2.4	5 cm/s
LT-E	C_2H_4	44.4	55.6	0.0	2.4	3 cm/s
HT-E	C_2H_4	44.4	55.6	0.0	2.4	4 cm/s
LT-B	C_6H_6	5.7	21.6	72.7	2	3 cm/s
HT-B	C_6H_6	5.7	21.6	72.7	2	4 cm/s

The notation of Russo *et al.* [14] is adopted here, where LT and HT indicate lower-temperature and higher-temperature flames, respectively. The flame temperature of the two flames with the same fuel and mixture composition is varied indirectly by changing the cold gas velocity. Increasing the velocity leads to lower heat losses to the burner and thereby to a higher temperature. As stated in [14], the difference in the peak temperature between the HT and LT cases is about 100 K. The measured temperature profiles have been imposed in the simulations. For the lower-temperature ethylene flame (LT-E) experimental temperature data were not available, and consequently, the profile for this flame was estimated based on the HT-E profile and the difference between the LT and HT flames for the other fuels.

The detailed chemical kinetic mechanism used for the simulations has been developed by Blanquart *et al.* [21] and further extended by Narayanaswamy *et al.* [22–24]. The mechanism describes the combustion of alkane fuels spanning from C_1 to C_8 as well as of substituted aromatic species such as benzene, toluene and xylene, and typical jet fuel surrogate components. Thus, the same mechanism could be used for all flames. Special emphasis in the development of the mechanism was placed on the accurate prediction of soot precursors. The mechanism has been extensively and successfully validated against experimental data measured in shock tubes, rapid compression machines, perfectly stirred reactors, and flow reactors, cf. [21] and references therein.

For each of the three fuels, the results for one of the flames are evaluated in Fig. 1, and similar observations hold for the other flames. Experimental data have been shifted by a few milliseconds to account for probe effects. As the experimental data are given in varying quantities, all data have been transferred into residence time and soot yield in [g soot/g fed carbon]. Required quantities for these calculations, such as the velocity and gas density, have been taken from the simulations. For all three flames, the soot yield is predicted with reasonable accuracy, cf. Fig. 1 (left column), the largest deviation by a factor of about three is observed for the methane flame.

By evaluating the predictions for the H/C ratio, it can be analyzed whether the relative contribution of the different soot formation mechanisms is plausible. For the correct prediction of the H/C ratio, the following two issues are very important: First, the relative importance of PAH-based growth, i.e. the sum of nucleation and condensation, and acetylene-based growth, also referred to as surface growth, must be correctly predicted. PAH-based growth moves the average H/C ratio towards the value of the H/C ratio of the nucleating or condensating PAH species (mostly this means that the H/C ratio is increased). Surface growth always reduces the H/C ratio as mostly carbon is added to the particles. Second, the average H/C ratio of the PAH species forming the soot particles has to be accurately predicted.

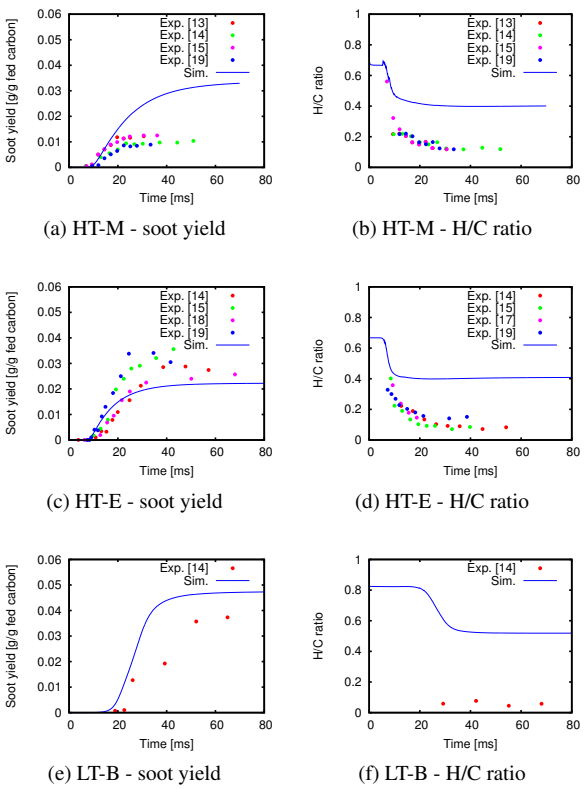

(a) HT-M - soot yield (b) HT-M - H/C ratio

(c) HT-E - soot yield (d) HT-E - H/C ratio

(e) LT-B - soot yield (f) LT-B - H/C ratio

Figure 1: Simulation results using the baseline model in terms of soot yield (left column) and H/C ratio (right column) for one of the methane (top row), ethylene (middle row) and benzene flames (bottom row). Experimental data from [13–15, 17–19].

The profiles for the H/C ratio are compared to experimental data in the right column of Fig. 1. Measurements are only available after the soot particles have started to grow and surface growth has become important. It is therefore difficult to evaluate whether the H/C ratio of the soot-forming PAH is well predicted. However, the most upstream data point of the measurements by Russo *et al.* [15] for the HT methane flame (cf. Fig. 1b) sug-

gests that the average H/C ratio of the freshly nucleated particles and hence of the soot forming PAH is around 0.6 or higher. In the simulations, the PAH species which contribute most to the dimerization and thus to the PAH-based growth, are acenaphthylene (A2R5) and biphenyl (P2), which have an H/C ratio of 0.667 and 0.833, respectively.

After about 10 ms, surface growth begins to become important, and the H/C ratio decreases rapidly in all flames. Qualitatively, this trend is captured by the model. However, in all flames, the absolute value of the H/C ratio in the post-flame region is overpredicted by at least a factor of three.

While the total soot mass is predicted well, the simulation results for the H/C ratio suggest that the fraction of the soot mass which is formed by PAH-based growth is too large compared to the soot mass which is formed by surface growth. This means that surface growth should be faster while PAH-based growth should be slower, such that the relative contribution of surface growth increases while the total soot mass growth remains the same.

The soot mass growth due to surface reactions depends on the reaction rates incorporated in the HACA mechanism and the concentration of acetylene. For the two methane flames and the HT ethylene flame, the profiles of the C_2H_2 mole fraction are compared to experimental data in Fig. 2. The very good agreement eliminates the possibility that the underprediction of the soot mass growth due to surface reactions is the result of underpredicted acetylene concentrations. It is therefore concluded that the surface growth rate should be increased in order to better predict the H/C ratio and the dehydrogenation process of soot particles in laminar premixed burner-stabilized flames.

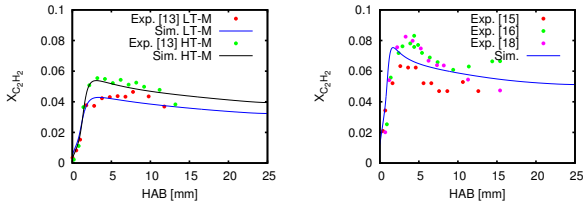

(a) LT-M and HT-M (b) HT-E

Figure 2: C_2H_2 mole fraction in the two methane flames and the HT ethylene flame. Experimental data from [13, 15, 16, 18].

4 Model improvements and simulation results using the updated model parameters

Following the analysis of the baseline simulation results discussed in the previous section, the sensitivity of the H/C ratio towards an increasing surface growth rate is studied first. It is anticipated that the soot yield, which is predicted well in the baseline simulations, will then be overpredicted, which gives rise to a correction of the PAH-based growth rate. Therefore, in the second part of this section, the impact of the coagulation efficiencies of PAH molecules to form dimers on the model predictions is evaluated. Finally, the simulations of the six flames are repeated with the updated surface growth rate and coagulation efficiencies. In addition, the updated model is tested for a larger set of laminar premixed ethylene flames.

4.1 Impact of soot surface growth rate on the H/C ratio

In order to evaluate the sensitivity of the H/C ratio to the relative contributions of the two growth processes, additional simulations of all six flames have been performed. For each flame, the surface growth rate has been multiplied by a constant factor ranging from 2 to 10. The PAH-based growth term has remained unchanged. For the three flames previously shown in Fig. 1, the results for the H/C ratio are compared to the baseline model predictions and the experimental data in Fig. 3. Again, the results for the other flames are very similar. The anticipated effect can be observed here. With increasing surface growth rate the H/C ratio is reduced to a lower value. The best results in terms of H/C ratio are obtained when the surface growth term is increased by a factor of 10.

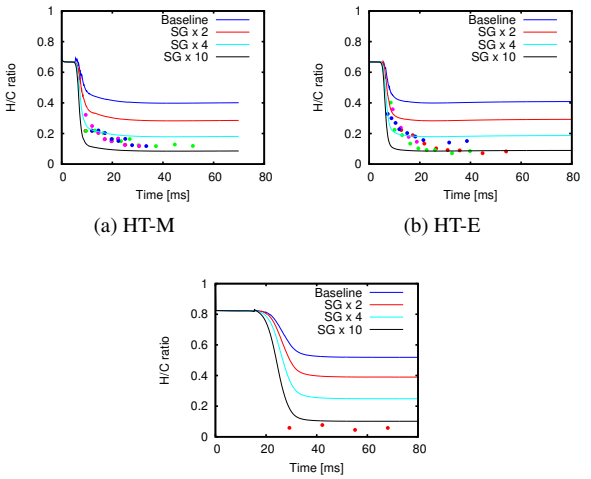

(a) HT-M (b) HT-E

(c) LT-B

Figure 3: Effect of increasing surface growth rate on the H/C ratio in the three flames previously shown in Fig. 1. Experimental data from [13–15, 17, 19], colors as in Fig. 1.

Of course, the soot yield is now overpredicted for the cases with higher surface growth rates (not shown here), which means that the model should predict an overall smaller amount of soot. This can be obtained by appropriately updating the coagulation efficiencies of the dimer production upon PAH collisions. Then, the surface growth rate and the dimer production rate need to be adjusted simultaneously, such that both the soot yield and the H/C ratio are in agreement with the experiments.

4.2 Impact of coagulation efficiencies on PAH concentrations

As explained in section 2, the soot nucleation and the PAH-based soot growth depend on the formation of dimers, which are formed when two PAH molecules collide. The coagulation efficiency of molecules or particles, i.e. the probability that the molecules stick together upon collision to form a dimer, increases exponentially with the size of the molecule, cf. [25, 26] and Table 1. However, the values suggested in the literature [25, 26] are somewhat lower than the coefficients applied in the

baseline model. This supports the need to reduce the coagulation efficiencies, which has been identified in the previous sections.

While the soot mass growth due to surface reactions is proportional to the surface growth rate, it should be noted that the effect of varying coagulation efficiencies on the soot mass growth due to PAH-based growth is very nonlinear. One reason is that the dimer formation rate depends on the square of the PAH concentrations. The PAH concentration profiles themselves are altered with varying coagulation efficiency. If the sticking efficiency is reduced, less PAH mass is transferred from the gas phase to the particulate phase in the upstream region, which leads to an increase of the PAH concentration further downstream. This in turn leads to an increase of the dimer formation rate in the downstream region.

For the HT ethylene flame, measurements of several PAH species are available [20]. In Fig. 4, the model predictions are compared to measurements of four species ranging from three-ringed to four-ringed PAH. Three cases are considered here: first, the baseline model; in a second case, all coagulation efficiencies are reduced by a factor of 10; in a third case, they are reduced by a factor of 100. Is is observed that the peak value of all concentrations increases by a factor of 5 to 10 when comparing the third case to the baseline model. In addition, the decrease in the post-flame region is reduced.

For all cases, the shape of the profile compares best to the experiments when the coagulation efficiencies are reduced by a factor of 100. The A2R5 concentration is overpredicted for the case with the lowest coagulation efficiency, but still in the correct order of magnitude. For the larger PAH species, the agreement with the experiments is very good for the case with the lowest coagulation efficiencies, only the pyrene concentration is slightly underpredicted.

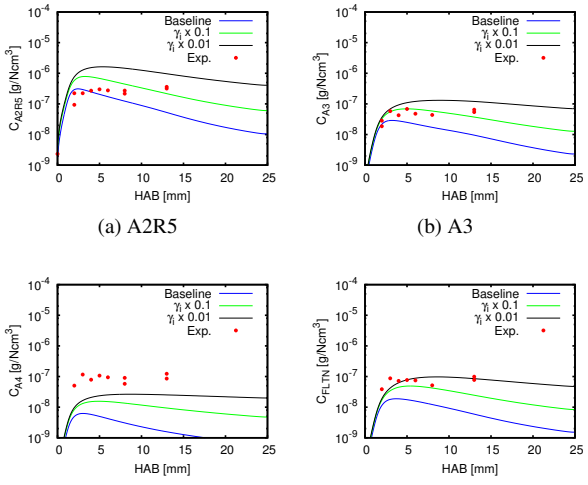

(a) A2R5 (b) A3

(c) A4 (d) FLTN

Figure 4: PAH concentrations for varying coagulation efficiencies in the HT ethylene flame. Experimental data from [20].

4.3 *Evaluation of H/C ratio and soot yield using the updated model parameters*

Simulations of the six flames listed in Table 2 are repeated with the updated model parameters. The surface growth rate is increased by a factor of 10, and the coagulation efficiencies are reduced by a factor of 100. Exemplarily, the profile of the H/C ratio in the LT benzene flame is depicted in Fig. 5a. The dehydrogenation of the soot particles is enhanced, since the relative contribution of acetylene-based soot growth compared to PAH-based soot growth is increased, and the model predictions compare favorably to the measurements.

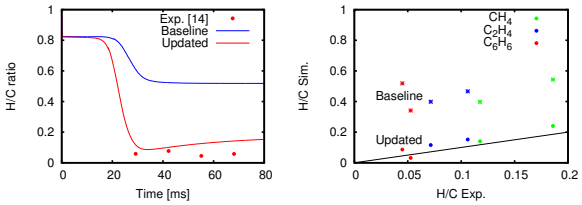

(a) LT-B (b) All flames listed in Table 2

Figure 5: H/C ratio in the LT benzene flame (left) and comparison of minimum H/C ratio between experiments and simulations in all flames listed in Table 2 (right). Experimental data from [14].

Figure 5b compares the model-predicted H/C ratio with the experiments for all flames listed in Table 2 in a more compact form. For both the baseline model and the updated model, the minimum H/C ratio obtained from the simulations is plotted against the experimental data. Ideally, all points should be located on the black line. As can be seen, the H/C ratio is decreased for the updated model, and the simulations can predict the dehydrogenation very well for all six flames.

To evaluate if the updated model still predicts the correct soot yield, the model-predicted soot yield is compared to the experimental value at the last measurement location in Fig. 6a. Overall, the agreement is good, as the deviation from the experimental values is less than a factor of three (indicated by the magenta lines) for the ethylene and benzene flames, and slightly higher for the methane flames. Compared to the baseline model, the accuracy of the predictions for the soot yield is virtually unchanged for all flames.

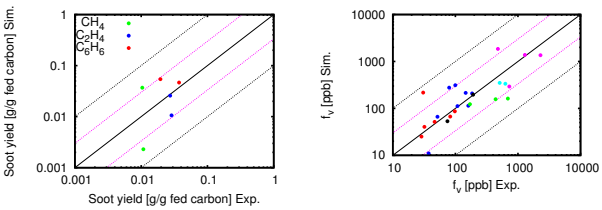

(a) Flames listed in Table 2 (b) ISF target flames

Figure 6: Model-predicted vs. measured soot yield for the flames listed in Table 2 (left) and for the ISF target flames (right). Experimental data from [14] (left) and [27] and references therein (right). Black solid line: perfect agreement between simulation and experiment; magenta lines: deviation by a factor of 3; black dotted lines: deviation by a factor of 10.

In addition to the six flames which have been used to determine the updated model parameters, the model is now tested for a larger set of laminar premixed ethylene flames. This set of flames has been suggested by the International Sooting Flame (ISF) Workshop [27] for soot model development and validation. The flames differ in terms of equivalence ratio, cold gas velocity and flame temperature. This results in the soot volume fraction spanning a range of two orders of magnitude.

The model-predicted results in terms of soot volume fraction are compared to the experimental data at the last measurement location in Fig. 6b. The soot volume fraction is predicted in the correct order of magnitude (indicated by the black dotted lines) for all flames, while for most of them, the deviation is less than a factor of three (indicated by the magenta lines).

5 Conclusions

A multivariate soot model based on the volume, surface area and number of hydrogenated sites on the surface of a soot particle has been applied to six burner-stabilized laminar premixed flames burning methane, ethylene, and benzene. To minimize the uncertainties in the results due to errors in the statistical model, MC simulations have been performed.

While the soot yield has been found to be in good agreement with the experiments, the H/C ratio has been overpredicted, meaning that the PAH-based growth is too dominant compared to the acetylene-based growth in the baseline model. A good agreement with the H/C ratio data could be obtained by increasing the surface growth rate. To compensate the increased soot yield due to increased surface growth, the coagulation efficiencies of the dimer formation were reduced, which also had a positive effect on the prediction of PAH species concentrations. The updated model was then validated for a larger set of laminar premixed flames including the six flames with H/C ratio data.

Acknowledgements

This work has been part of the project "DREAM-CODE" (grant no. 620143) within the Clean Sky Joint Undertaking, and corresponding funding by the European Union is gratefully acknowledged. In addition, the authors would like to thank Prof. Guillaume Blanquart for his help with the Monte Carlo simulation code and Dr. Carmela Russo for providing temperature data for the flames with H/C ratio measurements.

References

[1] U. O. Köylü, G. M. Faeth, T. L. Farias, M. G. Carvalho, Combust. Flame 100 (1995) 621–633.

[2] M. E. Mueller, G. Blanquart, H. Pitsch, Proc. Combust. Inst. 32 (2009) 785–792.

[3] G. Blanquart, H. Pitsch, Combust. Flame 156 (2009) 1614–1626.

[4] G. Blanquart, H. Pitsch, in: Combustion Generated Fine Carbonaceous Particles, H. Bockhorn, A. D'Anna, A. Sarofim, and H. Wang, Eds. KIT Scientific Publishing, pp. 439–466.

[5] M. Frenklach, H. Wang, Proc. Combust. Inst. 23 (1991) 1559–1566.

[6] M. Frenklach, Chem. Eng. Sci. 57 (2002) 2229–2239.

[7] A. Eibeck, W. Wagner, SIAM J. Sci. Comput. 22 (2000) 802–821.

[8] D. T. Gillespie, J. Atmos. Sci. 32 (1975) 1977–1989.

[9] M. Goodson, M. Kraft, J. Comput. Phys. 183 (2002) 210–232.

[10] R. I. A. Patterson, J. Singh, M. Balthasar, M. Kraft, W. Wagner, Combust. Flame 145 (2006) 638–642.

[11] J. Singh, R. Patterson, M. Balthasar, M. Kraft, W. Wagner, Modelling soot particle size distribution: Dynamics of pressure regimes, 2004. Preprint, University of Cambridge.

[12] H. Zhao, A. Maisels, T. Matsoukas, C. Zheng, Powder Technol. 173 (2007) 38–50.

[13] M. Alfè, B. Apicella, J.-N. Rouzaud, A. Tregrossi, A. Ciajolo, Combust. Flame 157 (2010) 1959–1965.

[14] C. Russo, M. Alfè, J.-N. Rouzaud, F. Stanzione, A. Tregrossi, A. Ciajolo, Proc. Combust. Inst. 34 (2013) 1885–1892.

[15] C. Russo, A. Tregrossi, A. Ciajolo, Proc. Combust. Inst. 35 (2015) 1803–1809.

[16] B. Apicella, R. Barbella, A. Ciajolo, A. Tregrossi, Combust. Sci. Technol. 174 (2002) 309–324.

[17] A. Ciajolo, R. Barbella, A. Tregrossi, L. Bonfanti, Symp. (Int.) Combust. 27 (1998) 1481–1487.

[18] A. Ciajolo, A. D'Anna, R. Barbella, A. Tregrossi, A. Violi, Symp. (Int.) Combust. 26 (1996) 2327–2333.

[19] M. Sirignano, M. Alfè, A. Tregrossi, A. Ciajolo, A. D'Anna, Proc. Combust. Inst. 33 (2011) 633–640.

[20] A. Ciajolo, A. Tregrossi, R. Barbella, R. Ragucci, B. Apicella, M. de Joannon, Combust. Flame 125 (2001) 1225–1229.

[21] G. Blanquart, P. Pepiot-Desjardins, H. Pitsch, Combust. Flame 156 (2009) 588–607.

[22] K. Narayanaswamy, G. Blanquart, H. Pitsch, Combust. Flame 157 (2010) 1879–1898.

[23] K. Narayanaswamy, P. Pepiot, H. Pitsch, Combust. Flame 161 (2014) 866–884.

[24] K. Narayanaswamy, H. Pitsch, P. Pepiot, Combust. Flame (2014). In Press.

[25] A. D'Alessio, A. C. Barone, R. Cau, A. D'Anna, P. Minutolo, Proc. Combust. Inst. 30 (2005) 2595–2603.

[26] A. Raj, M. Sander, V. Janardhanan, M. Kraft, Combust. Flame 157 (2010) 523–534.

[27] International Sooting Flame (ISF) Workshop, http://www.adelaide.edu.au/cet/isfworkshop/datasets/laminar/, 2014.